

# Calculation of molecular vibrational spectra on a quantum annealer

Alexander Teplukhin,<sup>1</sup> Brian K. Kendrick,<sup>1,\*</sup> and Dmitri Babikov<sup>2</sup>

<sup>1</sup>*Theoretical Division (T-1, MS B221),*

*Los Alamos National Laboratory, Los Alamos, New Mexico 87545, USA*

<sup>2</sup>*Department of Chemistry, Marquette University, Milwaukee, Wisconsin 53021, USA*

## Abstract

Quantum computers are ideal for solving chemistry problems due to their polynomial scaling with system size in contrast to classical computers which scale exponentially. Until now molecular energy calculations using quantum computing hardware have been limited to quantum simulators. In this paper, a new methodology is presented to calculate the vibrational spectrum of a molecule on a quantum annealer. The key idea of the method is a mapping of the ground state variational problem onto an Ising or quadratic unconstrained binary optimization (QUBO) problem by expressing the expansion coefficients using spins or qubits. The algorithm is general and represents a new revolutionary approach for solving the real symmetric eigenvalue problem on a quantum annealer. The method is applied to two chemically important molecules: O<sub>2</sub> (oxygen) and O<sub>3</sub> (ozone). The lowest two vibrational states of these molecules are computed using both a hardware quantum annealer and a software based classical annealer.

---

\* Correspondence should be addressed to BKK (bkendric@lanl.gov).

## INTRODUCTION

Quantum computers are seen by many as a future alternative to classical computers. Although quantum supremacy has not yet been achieved, the field is advancing quite rapidly. There are three major types of quantum computing devices (1): quantum annealer (2), quantum simulator (3–5), and a universal quantum computer. The first type is an example of adiabatic quantum computing (6) and is used to solve optimization problems, which at first glance appears to be quite restrictive. The second type is based on quantum gates which appears to have a wider applicability and therefore may be able to simulate a larger variety of problems. However, adiabatic and gate based quantum computing were proven to be formally equivalent (7). Thus, the practical application space is most likely limited by the hardware realization and not necessarily by the type of approach. The third type will be able to solve any problem but it does not yet exist. Building a universal quantum computer is a very challenging task and its realization may be decades away.

Coming from the physical chemistry community, we asked ourselves if it would be possible to program an important fundamental problem on a quantum annealer such as the commercially available D-Wave machine (8). Typically, people who work with such devices go in the opposite direction: knowing hardware capabilities they come up with a suitable optimization problem. As a fundamental problem we chose to calculate the vibrational ground state and possibly excited states of a molecule. This problem is very important in chemistry, for example:  $\text{H}_n^+$  ions (9–12),  $\text{CH}_5^+$  and isotopologues (13, 14),  $\text{H}_3\text{O}^+$ ,  $\text{H}_5\text{O}_2^+$  and deuterated analogues (15, 16), hydrogen clusters (17–19), their isotopologues (20, 21), hydrogen bonded systems (22) and Lennard-Jones clusters (23, 24). The common method to study these molecular systems is a Monte-Carlo (MC) method in its various flavors: variational MC, time-dependent variational MC, diffusion MC, and path integral MC.

A very similar ground state problem was addressed recently (25–27), where the authors designed an algorithm to calculate the electronic ground state on a quantum simulator. The result of their work is a Variational Quantum Eigensolver (VQE), where an expectation value of each term in the electronic Hamiltonian is evaluated on a trial wave function using a quantum simulator and the resultant total energy serves as a guide for generating the next trial wave function. The method is hybrid, because an optimization step, namely the trial generation, is performed on a classical computer.

In contrast to the VQE algorithm which is based on a quantum simulator, the new algorithm presented in this work is based on a quantum annealer and solves any real symmetric eigenvalue problem. To our knowledge, this is the first quantum annealer based eigenvalue solver and will be referred to below as the Quantum Annealer Eigensolver (QAE). As discussed in more detail below, our QAE algorithm is also hybrid since the variational eigenvalue problem is solved via a sequence of many quantum annealer optimizations performed with varying weights on the constraint equations (i.e., Lagrange multipliers). The scanning and optimization of the weights is done on a classical computer. Mapping the eigenvalue problem to a quantum annealer hardware is non-trivial, because the annealer solves a minimization problem defined by an Ising functional of the form  $H(s) = \sum_i h_i s_i + \sum_{i<j} J_{ij} s_i s_j$ , where the spin variables  $s_i$  accept values  $\{-1,1\}$ . Alternatively, the functional can be converted to quadratic unconstrained binary optimization (QUBO) form using variables  $x_i \in \{0,1\}$ , called qubits, giving  $H(x) = \sum_i Q_{ii} x_i + \sum_{i<j} Q_{ij} x_i x_j$  (28). The problem is how to write down a ground state or eigenvalue problem in QUBO form and explicitly construct the matrix  $\mathbf{Q}$ .

The outline of the paper is as follows: First, we present our solution to this problem, including the extension to the excited state calculations and multiple dimensions. Second, we apply our algorithm to two chemically important species,  $\text{O}_2$  (oxygen) and  $\text{O}_3$  (ozone). Third, the introduction of weighted constraints is presented following a technique used to overcome the connectivity issue in the quantum annealer hardware (i.e., D-Wave machine). Noise is also modeled in the algorithm which is shown to reproduce the results from the D-Wave machine. In the final discussion section, we consider possible improvements of the algorithm and sources of error.

## RESULTS

### Mapping of ground state problem to QUBO problem

The method is inspired by the variational principle. Suppose we are interested in a ground state of a one-dimensional system and its wave function  $\Psi$  is expanded using an orthonormal basis  $\varphi_\alpha$  and unknown expansion coefficients  $a_\alpha$ :  $\Psi = \sum_{\alpha=1}^B a_\alpha \varphi_\alpha$ . Then, the ground state energy can be expressed as a double sum over the Hamiltonian matrix elements

$E = \langle \Psi | \hat{H} | \Psi \rangle = \sum_{\alpha, \beta}^{B, B} a_{\alpha} a_{\beta} \langle \varphi_{\alpha} | \hat{H} | \varphi_{\beta} \rangle = \sum_{\alpha, \beta}^{B, B} a_{\alpha} a_{\beta} H_{\alpha\beta}$  It is easy to see that the functional form for the energy  $E$  is similar to QUBO form  $H(s)$ , except that the coefficients  $a_{\alpha}$  are continuous and  $a_{\alpha} \in [-1; 1]$  (since from the normalization condition  $\langle \Psi | \Psi \rangle = 1$  we know  $\sum_{\alpha=1}^B a_{\alpha}^2 = 1$ ). In contrast, the QUBO variables  $x_i$  are discrete.

The key idea in mapping the eigenvalue problem with Hamiltonian matrix  $\mathbf{H}$  to the QUBO optimization problem with matrix  $\mathbf{Q}$  is to express each expansion coefficient  $a_{\alpha}$  using  $K$  qubits  $q_k^{\alpha}$ . This approximation can be done in multiple ways. The approach we followed in this work is a fixed-point representation that is used to represent real numbers in a computer. Since the magnitude of the coefficients  $a_{\alpha}$  never exceeds unity, only the fractional part of the coefficient has to be stored. The last qubit  $q_K^{\alpha}$  stores the sign of  $a_{\alpha}$ . The complete expression for the coefficient is  $a_{\alpha} = \sum_{k=1}^{K-1} 2^{k-K} q_k^{\alpha} - q_K^{\alpha} \in [-1; 1)$ . Now, the functional  $E$  can be expressed explicitly in terms of the qubits  $q_k^{\alpha}$ . The powers of two are combined with the matrix elements  $H_{\alpha\beta}$  giving the matrix elements  $Q_{ij}$ . The qubits  $q_k^{\alpha}$  are mapped to the qubits  $x_i$  via the relation  $i = K(\alpha - 1) + k$ , where  $i \in [1, B \times K]$ . Since in the QUBO (or Ising) model the ordering of qubits within the pair does not matter (i.e., the interaction between  $i$  and  $j$  is the same as  $j$  and  $i$ ), the summation is restricted to  $i < j$  and the non-diagonal elements  $Q_{ij}$  are multiplied by two.

Unfortunately, the minimum of the functional  $E$  is a trivial solution  $\Psi = 0$ , which is due to the lack of the normalization constraint  $\|\Psi\| = 1$ . The workaround is to add that constraint right into the functional with a strength  $\lambda$ , giving  $I = \langle \Psi | \hat{H} | \Psi \rangle + \lambda(1 - \langle \Psi | \Psi \rangle)^2$ . Essentially, the parameter  $\lambda$  penalizes any deviation of the norm from unity and it helps to guide the optimization away from the trivial solution. One can think of  $\lambda$  as a Lagrange multiplier and the functionals  $E$  and  $I$  as objective functions. The problem with the functional  $I$  is that it is no more a QUBO functional, rather it is biquadratic in  $x$ . The trick is to lower the power of the constraint, giving  $G = \langle \Psi | \hat{H} | \Psi \rangle + \lambda(1 - \langle \Psi | \Psi \rangle)$ . Dropping the constant shift  $\lambda$ , which has no effect on the optimization, one obtains the final expression for the functional from used in present study:  $F = \langle \Psi | \hat{H} | \Psi \rangle - \lambda \langle \Psi | \Psi \rangle$ . The main consequence of the decreased power is that the normalization condition is broken *per se* (but this can be fixed by renormalizing the final solution). However, the primary role of the penalty is to avoid the trivial solution and the functional  $F$  serves that purpose. Another issue with the functional  $F$  is that it encourages a nonphysical norm  $\|\Psi\| > 1$ . This limits the number of techniques to find a good parameter  $\lambda$ . Ideally,  $\lambda$  should be large enough to kick the

optimization away from the trivial solution minimum but yet small enough to stay away from the large norm limit. To find an optimal value for  $\lambda$ , we scan in  $\lambda$  and pick the solution with the lowest energy  $E = \langle \Psi | \hat{H} | \Psi \rangle$  (where here  $\Psi$  has been renormalized:  $\langle \Psi | \Psi \rangle = 1$ ).

### Calculation of excited states

The QAE algorithm described above can be easily applied to the calculation of excited states by modifying the initial Hamiltonian  $\mathbf{H}$ . Specifically, for the first excited state, an outer product matrix of the previously computed ground state wave function is added:  $\mathbf{H}' = \mathbf{H} + S_0 |\Psi_0\rangle\langle\Psi_0|$ . The parameter  $S_0$  is an arbitrary user specified energy shift to move the ground state higher in the spectrum. The only requirement on  $S_0$  is that it should be larger than the energy of the first excited state, otherwise the algorithm will keep converging to the ground state. To compute the  $i$ -th excited state, similar terms for the states  $0, \dots, (i-1)$  should be added to the Hamiltonian. In principle, this iterative procedure allows one to compute the whole spectrum of a molecule. Obviously, for a fixed basis size  $B$  and qubit expansion  $K$ , the higher states will not be described as accurately as the lower ones.

### Multiple dimensions

The generalization of the QAE method to multiple dimensions is straightforward. For a direct product basis, the one-dimensional expansion is replaced with an  $n$ -dimensional expansion, but the way to code each expansion coefficient using  $K$  qubits remains the same. For example, for a two-dimensional system with the same number of basis functions  $B$  for each dimension, the expansion is  $\Psi = \sum_{\alpha,\beta}^{B,B} a_{\alpha\beta} \varphi_\alpha \theta_\beta$ , where  $\varphi_\alpha$  and  $\theta_\beta$  are the basis functions in each dimension. The qubits  $q_k^{\alpha\beta}$  are now mapped to the variables  $x_i$  as follows:  $i = KB(\alpha - 1) + K(\beta - 1) + k$ , where  $i \in [1, B^2 \times K]$ .

The QAE method can also be applied to a non-direct product basis. For example, one can implement a Sequential Diagonalization Truncation (SDT) (29–31) which drastically reduces the size of the Hamiltonian matrix and ultimately results in a much smaller total number of qubits than in direct product treatment. We use the SDT approach for ozone and further details of applying the SDT method to that molecule can be found elsewhere(32).

## Application to O<sub>2</sub> and O<sub>3</sub>

We applied our algorithm to the calculation of the ground and first excited states of the oxygen and ozone molecules. For both, we used an accurate potential energy surface of ozone (33). The one-dimensional O<sub>2</sub> potential  $V(r_{\text{O}_2})$  was generated from the full three-dimensional ozone potential by moving one of the oxygen atoms far away from the other two (i.e.,  $R_{\text{O-O}_2} = 60 a_0$ ). The two lowest wave functions for both molecules are shown in Fig. 1. The software based classical QUBO solver reproduces the wave functions computed with a standard classical numerical eigensolver (LAPACK (34)), whereas the output of the hardware quantum annealer (D-Wave machine) is less accurate. The sharp edges (low resolution) of the wave functions is due to the small size of the basis set. For oxygen, a Fourier basis ( $e^{imr_{\text{O}_2}}$ ) was chosen small enough to give the known ground state energy of 791.64 cm<sup>-1</sup> within an error of 0.01 cm<sup>-1</sup> using a standard classical numerical eigensolver (LAPACK). The required number of periods in the Fourier series is  $m_{\text{max}} = 4$  which translates to the basis size  $B = 2m_{\text{max}} + 1 = 9$ . For ozone, an accurate calculation would require significant computational resources, so we decided to use an SDT basis set truncated at quite low energy  $E_{\text{cut}} = 2000$  cm<sup>-1</sup>, which gives  $B = 12$  basis functions. This basis is sufficient to describe the ground state at 1451 cm<sup>-1</sup> with an error of 120 cm<sup>-1</sup> using LAPACK, but is too small for excited state calculations (the computed excited state energy is 700 cm<sup>-1</sup> larger than the true value of 2147 cm<sup>-1</sup>). Nevertheless, in this work we are primarily interested in benchmarking the new QAE method against a standard classical numerical eigensolver (LAPACK) and not in the absolute accuracy of the solutions. We refer the reader interested in accurate classical calculations to the relevant literature (32, 35). For the three-dimensional ozone system, we plot the probability density (the wave function squared) as a function of the symmetric-stretch coordinate  $\rho$  in Fig. 1b (36, 37). The SDT basis functions span the other two internal degrees of freedom (not plotted) at each value of  $\rho$  and are computed classically (32). The number of qubits  $K$  per expansion coefficient (or basis function) is 7 for oxygen and 5 for ozone which is the maximum possible number which fits within the 64 logical fully-connected qubits on the hardware quantum annealer (D-Wave machine). Namely,  $K \cdot B = 7 \cdot 9 = 63$  for oxygen and  $K \cdot B = 5 \cdot 12 = 60$  for ozone.

Figure 2 illustrates the convergence of the energies as a function of the number of qubits  $K$  per expansion coefficient  $a_\alpha$  (i.e., the level of discretization). There are several interesting

findings to discuss. First, the error decreases exponentially as a function of  $K$ , which is very appealing. Second, the error decreases and reaches a plateau, for both solvers and both systems. This shared behavior demonstrates that the QAE algorithm itself is universal, but the actual error is solver and system dependent. Third, the quantum annealer (D-Wave machine) is much less accurate (by two-three orders of magnitude) than the classical QUBO solver. In addition, because the total number of qubits currently available in the quantum annealer is rather limited, the corresponding (dashed) curves do not continue to higher values of  $K$ . Finally, the classical QUBO solver brings the error for  $O_2$  down to  $0.01 \text{ cm}^{-1}$  which coincidentally matches the error of chosen basis size. No more than  $K = 8$  qubits (a qubyte) per coefficient are needed for oxygen. For ozone,  $K = 5$  qubits are required by the classical QUBO solver to reach the plateau within an error of less than  $3 \text{ cm}^{-1}$ . This is quite accurate, compared to the  $120 \text{ cm}^{-1}$  error due to the chosen (small) SDT basis.

Table S1 in Supplementary Materials gives the parameters used in scanning over the normalization penalty  $\lambda$ . The initial  $\lambda_{min}$  could be zero or some value that is smaller than the expected energy of the state being computed (if it is known). The number of steps  $N_\lambda$  specifies the number of samples and is a convergence parameter. The last parameter is the step size  $\Delta\lambda$  which ideally should be the same for all  $K$  within a given problem. However, for small  $K$  we were always getting trivial solutions which is probably due to the inaccurate description of the problem. The only way we found to avoid this is to increase the step size  $\Delta\lambda$  by more than an order of magnitude. We faced the same issue when we were simulating the hardware noise. Increasing both the step size and the number of steps allowed us to overcome this obstacle.

### Algorithm scaling

It is straightforward to show that the runtime scales as  $O(N_\lambda K B^d)$ , where  $d$  is the number of dimensions and  $B$  basis functions are used for each dimension. In practice, however, the QUBO solver may also have some additional (internal) effects on performance. For example, the classical QUBO solver we used in this work is based on a backbone-based method inspired by Glover, *et al.* (38) to partition the problem, which is causing a step-like runtime as a function of  $K$  (see Figure S1 in Supplementary Materials). In the next paragraph, we will show that the actual computational time is in agreement with the

theoretical scaling for the  $d$ -dimensional harmonic oscillator problem solved using a cosine basis and the classical QUBO solver. The oscillator frequencies were set different according to  $\omega_i(\text{cm}^{-1}) = 800 + 200 \cdot (i - 1)$ , where  $i$  is the dimension index. The linear scaling with  $N_\lambda$  is obvious.

To verify the linear scaling with  $K$ , we plot the normalized computational time divided by  $K$  as a function of  $K$  in Figure 3. As expected, all curves are horizontal and their slope does not depend on dimensionality (except for perhaps  $d = 5$ ). The rapid increase or steps at  $K = 16$  for 1D, at  $K = 6$  for 2D and at  $K = 2$  for 3D are due to partitioning size. They appear as soon as the total number of qubits exceeds the sub-QUBO size of 47, which is  $3 \times 16$  for 1D,  $3^2 \times 6$  for 2D and  $3^3 \times 2$  for 3D. Once the linear dependence on  $K$  has been established (see Fig. 3), one can then verify the exponential dependence on dimensionality  $d$ . The logarithm of the normalized computational time is plotted in Figure 4 as a function of the dimensionality  $d$ . All of the curves exhibit a linear dependence on  $d$  which confirms the exponential scaling. Again, the times for all  $K$  at  $d = 1$  and for  $K = 4$  at  $d = 2$  deviate significantly from the main trend because no partitioning is required to compute those. The average slope calculated based on  $d = 2$  through 4 is 0.58 which is close to the theoretically predicted value of 0.48 (for  $B = 3$ ). When  $d = 5$  is included the slope increases to 0.72 which is most likely due to the very large problem size. The total number of qubits for  $d = 5$  is  $KB^d = 972$  to  $3888$  for  $K = 4$  to  $16$  and  $B = 3$  which results in a total number of configurations  $10^{300}$  to  $10^{1000}$ . In summary, Figures 3 and 4 confirm the general scaling law  $O(N_\lambda KB^d)$  of the algorithm and any deviations from it are due to a particular QUBO solver.

We did not perform scaling studies on the hardware quantum annealer (D-Wave machine) because it was not practical due to the small number of logical qubits and long runtime. For example, for  $\text{O}_2$  we were able to approach small problems with  $B = 9$  and  $K = 1$  to  $7$  and the runtime was about  $t_{dw} = 2500$  s. This time does not depend on the number of logical qubits  $K$ , because all problems are treated by the hardware as maximum-size problems. In contrast, the classical QUBO solver runtime for these problems was about  $t_{cl} = 30$  s, which is almost two orders of magnitude smaller. The long runtime for the hardware quantum annealer is primarily due to the large number of reads (see Fig. S3). In addition, the analysis for the  $d$ -dimensional harmonic oscillator would require an extensive QUBO partitioning, which means another factor of ten to hundred increase in  $t_{dw}$ .



## Chaining in quantum annealer

The only constraint we have discussed so far is a normalization constraint with associated penalty  $\lambda$ . However, there is another constraint and penalty factor worth mentioning when running on a quantum annealer (D-Wave machine). Namely, the chain constraint and the associated chain penalty. The physical qubits in the hardware do not have an all-to-all connectivity which is a requirement of the algorithm. In fact, each qubit has six neighbors at most (see Chimera graph) (28). Fortunately, there is a method to embed a fully connected graph on top of the hardware graph. In this approach, a number of qubits are organized into so-called chains. Qubits within a chain act like a single logical qubit which is connected to all other logical qubits. To program chains in the hardware Chimera graph, one adds a set of constraints which have a single strength or chain penalty  $c$ . As with any constraint, the associated penalty or weight  $c$  should be neither too small, because then the chains are broken, or too large, because then the hardware will become insensitive to the original problem. The simplest approach to find a good chain penalty is to perform scanning, in a similar way to  $\lambda$  scanning. Figure 5 demonstrates an example of this two-dimensional scanning for the ground state of  $O_2$  with a Fourier basis of size  $B = 7$  ( $m_{max} = 3$ ) and  $K = 3$ . As expected, in the region of small  $c$  the minimum energy is unacceptably large, simply due to broken chains. For large  $c$  we see two regions: the region of small  $\lambda$ , which contains trivial solutions only (because the normalization constraint is too weak) and the region of large  $\lambda$  with reasonable minimum energies. The phase transition between these two regions occurs close to the true ground state energy  $791.64 \text{ cm}^{-1}$ . The result of this two-dimensional scanning shows that a reasonable chain penalty lies between 10000 - 20000  $\text{cm}^{-1}$ . We used  $c = 15000 \text{ cm}^{-1}$  in all of our calculations.

## Simulating hardware noise

The results obtained on the quantum annealer are much less accurate than those obtained using the classical QUBO solver (see Figures 1 and 2). We believe that this discrepancy is partially due to the error with which the QUBO problem is programmed in the hardware. The reported integrated control errors (ICE) for the hardware we used are quite large (8). For example, the diagonal elements are programmed with a mean error 0.7% of the maximum

matrix element. In the  $\text{O}_2$  calculation, the maximum matrix element is  $11.5 \times 10^3 \text{ cm}^{-1}$  which translates into an ICE of  $80 \text{ cm}^{-1}$ . Moreover, the error has a quite broad distribution, its standard deviation is 0.8%. This can potentially double the ICE, bringing it to  $160 \text{ cm}^{-1}$ . Upon consideration of this source of error, the large difference between the quantum annealer and classical results in Figure 2 is no longer that surprising. To quantify the effects of the hardware errors (noise), we performed calculations with a classical solver where random noise was manually added to QUBO (see Materials and Methods). The errors (relative to LAPACK) of the classical QUBO solutions with different magnitudes of noise are shown in Figure 6. On average, introduction of noise increases the error. For the 1D harmonic oscillator, the default noise (using the reported ICE values discussed above) mimics the quantum annealer behavior. For oxygen, the quantum annealer behavior is well characterized if the noise is increased by a factor of three. For ozone, a factor of 5 or 7 is enough. As the problem size increases, larger noise scaling is required (to mimic the hardware performance), which implies that there could be some other source of discrepancy between the hardware and software solvers. Also, introduction of noise required an increase in the strength of the normalization weight  $\lambda$  which is reflected in Table S1.

## DISCUSSION

There are several places in the method where some improvements could be done and which are definitely worth listing. First, the functional form we used in this study is not the only one. For example, the initial biquadratic functional  $I$ , that we simplified earlier, can be converted to a quadratic QUBO form using multiple additional constrains. The drawback of this approach is that it will require additional penalty factors and ultimately will make the problem much harder to manage and solve.

Second, the method would significantly benefit if the normalization condition could be integrated into the functional, rather than added to it. For example, one can notice that solution  $\mathbf{a}$  represents a point on the unit hypersphere. Thus, its position can be described using spherical coordinates and the angles could be approximated with qubits  $\mathbf{q}$ . However, the presence of products of sines and cosines in this kind of mapping results in a polynomial of high degree in  $q$ . This would require multiple constraints and associated penalty factors to convert the problem into quadratic form. The problem becomes difficult again.

Third, the actual scaling of the algorithm depends on the solver and its parameters. For the classical QUBO solver used in this work, the stopping criterion is specified by the number of repeats without any improvement. For the quantum annealer, the user specifies the number of annealing cycles or reads (see Materials and Methods). The scaling we discussed earlier is for the algorithm itself which excludes internal scaling effects of a particular QUBO solver.

Fourth, the physical or working Chimera graph of the quantum annealer is not perfect. The yield of the working graph, the percentage of working qubits (and couplers) that are present, is 99% (98%) (8). To make it a full-yield graph, an additional software post-processing is performed before results are sent back to the user. The user may opt out of this fixing procedure, however, that reduces portability of the algorithm, since every machine has its own working graph. Still removing this layer might be worth exploring.

Fifth, the annealing time  $t_{ann}$  is another parameter that can potentially play some role in the annealing process. We found that increasing  $t_{ann}$  does not change results significantly. What affects the results more was the number of reads  $N_{reads}$ . Because there is a limitation  $t_{ann} \cdot N_{reads} < 3$  seconds in the API, we chose the maximum number of reads per job submission:  $N_{reads} = 10^4$  and  $t_{ann} = 299 \mu\text{s}$ . The maximum allowed  $t_{ann}$  is  $2000 \mu\text{s}$  but it would be good to explore larger annealing times if possible.

Sixth, it is not quite clear how to properly include the ICEs in the noise simulation tests. The errors are reported solely for the maximum and minimum elements of QUBO matrix and they are a function of annealing time. In addition, they were reported for 70% of the annealing process (i.e., there is no error data at the end of annealing) (8). For the noise tests reported in this work, we used the reported errors at 70% and manually scaled them.

Seventh, the annealer temperature could be another source of error. In a recent paper (39) it was argued that the annealer temperatures must be appropriately scaled down with problem size (at least in a logarithmic way or better yet as a power law). In fact, during our study we had to switch from the device with 1024 qubits (DW2X) to 2048 qubits (DW2000Q). The temperature lowered from 15.7 mK to 14.5 mK, which is almost logarithmic (it should be 14.3 mK). However, we had to perform 50 times more reads on the larger machine to reproduce trivial solutions for small  $\lambda$  and large  $c$ .

Finally, the landscape of the hypothetical configuration space is defined by the problem. It could be that our problems have high and thick barriers on the landscape, which effec-

tively disables the tunneling mechanism in the annealer and restricts exploration. Another possibility is that the landscape has a large number of wells and the solver jumps from one to another. Possibly, a very long annealing time could help to determine if this is the case.

In summary, we developed a hybrid algorithm (QAE) for the calculation of the vibrational spectrum of a molecule on a quantum annealer. The eigenvalue problem is mapped to the QUBO (Ising) problem by discretization of the expansion coefficients using qubits. The method is hybrid due to the scanning in a penalty (or weight) to impose wave function normalization. Running on the actual quantum annealer requires the additional scanning in chain penalty. The method was applied to the ground and first excited vibrational states of two chemically important species:  $O_2$  (oxygen) and  $O_3$  (ozone). The QAE calculations based on the classical QUBO solver outperform those on the quantum annealer (D-Wave machine) in both accuracy and computational time (i.e., no supremacy of the latter one). Our tests show that this is partially due to the errors or noise present in the hardware. Hopefully, in the future it will be possible to build larger, more accurate and fully-connected quantum annealers. As a final note, the QAE algorithm is universal and can be used in any field of science or engineering to solve the real symmetric eigenvalue problem.

## MATERIALS AND METHODS

We used qbsolv (40) as the software classical QUBO solver and the D-Wave 2000Q (8) as the hardware quantum solver. The underlying qbsolv algorithm is a combination of Tabu search and a backbone-based method inspired by Glover *et al.* (38). The latter one is used for partitioning the original (large) QUBO into smaller sub-QUBOs. The only modification we did was to increase the span of partitioning to 1 (the hard-coded value is 0.214). The number of repeats in the stopping criterion is  $N_{rep} = 10^4$ . For the excited states calculations we used  $S_0 = 9000 \text{ cm}^{-1}$ , however 3000 and 6000 also worked well.

The hardware was accessed using qOp stack: qbsolv, DW library and SAPI (41). Although qbsolv allows running sub-QUBOs on the hardware, we did not follow this approach, because the contribution of the D-Wave machine to the solution would be hard to estimate. Furthermore, qbsolv does implicit restarts and uses a classical Tabu search to refine solutions. Thus, a hardware calculation using the default qbsolv is actually hybrid and not fully quantum (for problems that fit one sub-QUBO qbsolv is completely classical). In order to

bring the actual D-Wave performance to the surface, we removed partitioning, restarts and refinement from qbsolv, so that it only serves as an interface to the hardware. In addition, we raised the number of reads to  $10^5$  (the hard-coded value is 25). Figure 5 was prepared with  $5 \times 10^5$  reads (half a million) and the chain penalty was  $15000 \text{ cm}^{-1}$  (the hard-coded value is 15). The number of physical qubits on the DW2000Q is 2028 qubits (99% yield) and 5903 couplers (98% yield). However, embedding a fully connected graph leaves us with just 64 logical qubits.

Our code generates input QUBO matrices for qbsolv. It is written in Fortran and uses LAPACK (34) as the classical numerical eigensolver (for benchmarking the QUBO results). Convergence studies were done for  $N_{rep}$ ,  $N_{reads}$  and  $N_\lambda$  and are reported in Figures S2-S4 of Supplementary Materials. We did not see a strong dependence on Tabu memory, so we used the default values. In addition, we tested the code on  $d = 1$  to 5 dimensional harmonic oscillators and the convergence for  $d = 1$  to 3 in terms of number of qubits  $K$  is given in Figure S5.

## REFERENCES

---

1. Ladd, T. D., Jelezko, F., Laflamme, R., Nakamura, Y., Monroe, C. and O'Brien, J. L. Quantum computers. *Nature*, **464**, 45–53 (2010).
2. Johnson, M. W., Amin, M. H., Gildert, S., Lanting, T., Hamze, F., Dickson, N., Harris, R., Berkley, A. J., Johansson, J., Bunyk, P. & Chapple, E. M. Quantum annealing with manufactured spins. *Nature*, **473**, 194–198(2011).
3. Geller, M. R., Martinis, J. M., Sornborger, A. T., Stancil, P. C., Pritchett, E. J., You, H. & Galiutdinov A. Universal quantum simulation with prethreshold superconducting qubits: Single-excitation subspace method. *Phys. Rev. A*, **91**, 062309 (2015).
4. Aspuru-Guzik, A., Dutoi, A. D., Love, P. J. & Head-Gordon, M. Simulated Quantum Computation of Molecular Energies. *Science*, **309**, 1704–1707 (2005).
5. Buluta, I. & Nori, F. Quantum Simulators. *Science*, **326**, 108–111 (2009).
6. Albash, T. & Lidar, D. A. Adiabatic quantum computation. *Rev. Mod. Phys.*, **90**, 015002 (2018).
7. Mizel, A., Lidar, D. A. & Mitchell, M. Simple Proof of Equivalence between Adiabatic Quantum Computation and the Circuit Model. *Phys. Rev. Lett.*, **99**, 070502 (2007).
8. D-Wave Systems Inc. QPU Properties: D-Wave 2000Q Online System (DW\_2000Q\_3). *User Manual*, 09-1180A-A (2018).
9. Lin Z. & McCoy A. B. Signatures of large-amplitude vibrations in the spectra of H5+ and D5+. *J. Phys. Chem. Lett.*, **3**, 3690–3696 (2012).
10. Lin Z. & McCoy A. B. Investigation of the structure and spectroscopy of H5+ using diffusion Monte Carlo. *J. Phys. Chem. A*, **117**, 11725–11736 (2013).
11. Qu, C., Prosimiti, R. & Bowman, J. M. MULTIMODE calculations of the infrared spectra of H+7 and D+7 using ab initio potential energy and dipole moment surfaces. In: Wilson A., Peterson K., Woon D. (eds) Thom H. Dunning, Jr. Highlights in Theoretical Chemistry, **10**, 141–147 (Springer, Berlin, Heidelberg, 2015)
12. Qu C. & Bowman J. M. Diffusion Monte Carlo calculations of zero-point structures of partially deuterated isotopologues of H7+. *J. Phys. Chem. B*, **118**, 8221–8226 (2014)

13. McCoy, A. B., Braams, B. J., Brown, A., Huang, X., Jin, Z., & Bowman, J. M. Ab initio diffusion Monte Carlo calculations of the quantum behavior of CH<sub>5</sub><sup>+</sup> in full dimensionality. *J. Phys. Chem. A*, **108**, 4991–4994 (2004).
14. Huang, X., Johnson, L. M., Bowman, J. M., & McCoy, A. B. Deuteration effects on the structure and infrared spectrum of CH<sub>5</sub><sup>+</sup>. *J. Am. Chem. Soc.*, **128**, 3478–3479 (2006).
15. Petit, A. S. & McCoy, A. B. Diffusion Monte Carlo approaches for evaluating rotationally excited states of symmetric top molecules: application to H<sub>3</sub>O<sup>+</sup> and D<sub>3</sub>O<sup>+</sup>. *J. Phys. Chem. A*, **113**, 12706–12714 (2009).
16. Guasco, T. L., Johnson, M. A. & McCoy, A. B. Unraveling anharmonic effects in the vibrational predissociation spectra of H<sub>5</sub>O<sub>2</sub><sup>+</sup> and its deuterated analogues. *J. Phys. Chem. A*, **115**, 5847–5858 (2011).
17. Rama Krishna, M. V. & Whaley, K. B. Structure of small molecular hydrogen clusters. *Z. Phys. D*, **20**, 223–226 (1991).
18. Warnecke, S., Sevryuk, M. B., Ceperley, D. M., Toennies, J. P., Guardiola, R. & Navarro, J. The structure of para-hydrogen clusters. *Eur. Phys. J. D*, **56**, 353–358 (2010).
19. Navarro, J. & Guardiola, R. Thermal effects on small parahydrogen clusters. *Int. J. Quantum Chem.*, **111**, 463–471 (2011).
20. Scharf, D., Martyna, G. J. & Klein, M. L. Isotope effect on the melting of para-hydrogen and ortho-deuterium clusters. *Chem. Phys. Lett.*, **197**, 231–235 (1992).
21. Cuervo, J. E. & Roy, P.-N. On the solid- and liquidlike nature of quantum clusters in their ground state. *J. Chem. Phys.*, **128**, 224509 (2008).
22. Curotto, E. & Mella, M. Quantum Monte Carlo simulations of selected ammonia clusters (n=2-5): Isotope effects on the ground state of typical hydrogen bonded systems. *J. Chem. Phys.*, **133**, 214301 (2010).
23. Noya, E. G. & Doyea, J. P. K. Structural transitions in the 309-atom magic number Lennard-Jones cluster. *J. Chem. Phys.*, **124**, 104503 (2006).
24. Deckman, J., Frantsuzov, P. A., & Mandelshtam, V.A. Quantum transitions in Lennard-Jones clusters. *Phys. Rev. E*, **77**, 052102 (2008).
25. Peruzzo, A., McClean, J., Shadbolt, P., Yung, M.-H., Zhou, X.-Q., Love, P. J., Aspuru-Guzik, A., & O’Brien, J. L. A variational eigenvalue solver on a photonic quantum processor. *Nat. Commun.* **5**, 4213 (2014).

26. McClean, J. R., Romero, J., Babbush, R. & Aspuru-Guzik, A. The theory of variational hybrid quantum-classical algorithms. *New J. Phys.*, **18**, 023023 (2016).
27. O’Malley, P. J. J. , Babbush, R., Kivlichan, I. D., Romero, J., McClean, J. R., Barends, R., Kelly, J., Roushan, P., Tranter, A., Ding, N., Campbell, B., Chen, Y., Chen, Z., Chiaro, B., Dunsworth, A., Fowler, A. G., Jeffrey, E., Lucero, E., Megrant, A., Mutus, J. Y., Neeley, M., Neill, C., Quintana, C., Sank, D., Vainsencher, A., Wenner, J., White, T. C., Coveney, P. V., Love, P. J., Neven, H., Aspuru-Guzik, A. & Martinis, J. M. Scalable quantum simulation of molecular energies. *Phys. Rev. X*, **6**, 031007 (2016).
28. D-Wave Systems Inc. Programming with QUBOs. *Tech. Report*, Release 2.4, 09-1002A-C (2017).
29. Bačić, Z. & Light, J. C. Highly excited vibrational levels of floppy triatomic molecules: A discrete variable representation—Distributed Gaussian basis approach. *J. Chem. Phys.* **85**, 4594–4604 (1986).
30. Light, C. & Bačić, Z. Adiabatic approximation and nonadiabatic corrections in the discrete variable representation: Highly excited vibrational states of triatomic molecules. *J. Chem. Phys.* **87**, 4008–4019 (1987).
31. Bačić, Z. & Light, J. C. Accurate localized and delocalized vibrational states of HCN/HNC. *J. Chem. Phys.*, **86**, 3065–3077 (1987).
32. Teplukhin, A. & Babikov D. Efficient method for calculations of ro-vibrational states in triatomic molecules near dissociation threshold: Application to ozone. *J. Chem. Phys.*, **145**, 114106 (2016).
33. Dawes, R., Lolur, P., Li, A., Jiang, B. & Guo, H. Communication: An accurate global potential energy surface for the ground electronic state of ozone. *J. Chem. Phys.*, **139**, 201103 (2013).
34. Anderson, E., Bai, Z., Bischof, C., Blackford, S., Demmel J., Dongarra, J., DuCroz, J., Greenbaum, A., Hammerling, S., McKenney, A., Sorensen, D. LAPACK Users’ Guide. (SIAM: Philadelphia, 1999, 3rd ed.).
35. Ndengué, S., Dawes, R., Wang, X.-G., Carrington, T. Jr., Sun, Z. & Guo, H. Calculated vibrational states of ozone up to dissociation. *J. Chem. Phys.*, **144**, 074302 (2016).
36. Teplukhin, A. & Babikov D. Interactive tool for visualization of adiabatic adjustment in APH coordinates for computational studies of vibrational motion and chemical reactions. *Chem. Phys. Lett.*, **614**, 99–103 (2014).



37. Teplukhin, A. & Babikov D. Visualization of Potential Energy Function Using an Isoenergy Approach and 3D Prototyping. *J. Chem. Educ.*, **92**, 305–309 (2015).
38. Wang, Y., Lü, Z., Glover, F., Hao, J.-K. A Multilevel Algorithm for Large Unconstrained Binary Quadratic Optimization. In: Beldiceanu N., Jussien N., Pinson . (eds) Integration of AI and OR Techniques in Constraint Programming for Combinatorial Optimzation Problems. CPAIOR 2012. Lecture Notes in Computer Science, **7298**. (Springer, Berlin, Heidelberg, 2012)
39. Albash, T., Martin-Mayor, V., & Hen, I. Temperature scaling law for quantum annealing optimizers. *Phys. Rev. Lett.* **119**, 110502 (2017). Code is available at <https://github.com/dwavesystems/qbsolv>
40. D-Wave Systems Inc. Partitioning Optimization Problems for Hybrid Classical/Quantum Execution. *Tech. Report*, 14-1006A-A (2017).
41. D-Wave Systems Inc. qOp toolset 2.5.1. Available from: <https://www.dwavesys.com> (accessed September 2018).

## ACKNOWLEDGEMENTS

**Funding:** A.T. and B.K.K. acknowledge that this work was done under the auspices of the US Department of Energy under Project No. 20170221ER of the Laboratory Directed Research and Development Program at Los Alamos National Laboratory. Los Alamos National Laboratory is operated by Los Alamos National Security, LLC, for the National Security Administration of the US Department of Energy under contract DE-AC52-06NA25396. We thank D-Wave Systems Inc. for providing access to the DW2X device at LANL and the DW2000Q device in Burnaby, Canada. A.T. thanks LANL for sponsoring his summer visit in 2017. D.B. acknowledges that this material is based upon work supported by the National Science Foundation under Grant No. AGS-1252486. **Author contributions:** A.T. developed the algorithm, performed the numerical calculations, analysis and writing of the manuscript. B.K.K. contributed to the development of the algorithm, analysis and writing of the manuscript. D.B. contributed to the analysis and writing of the manuscript. **Competing Interests:** The authors declare that they have no competing interests. **Data and materials availability:** All data needed to evaluate the conclusions in the paper are present in the paper and/or the Supplementary Materials. Additional data related to this paper may be requested from the authors.

## FIGURES

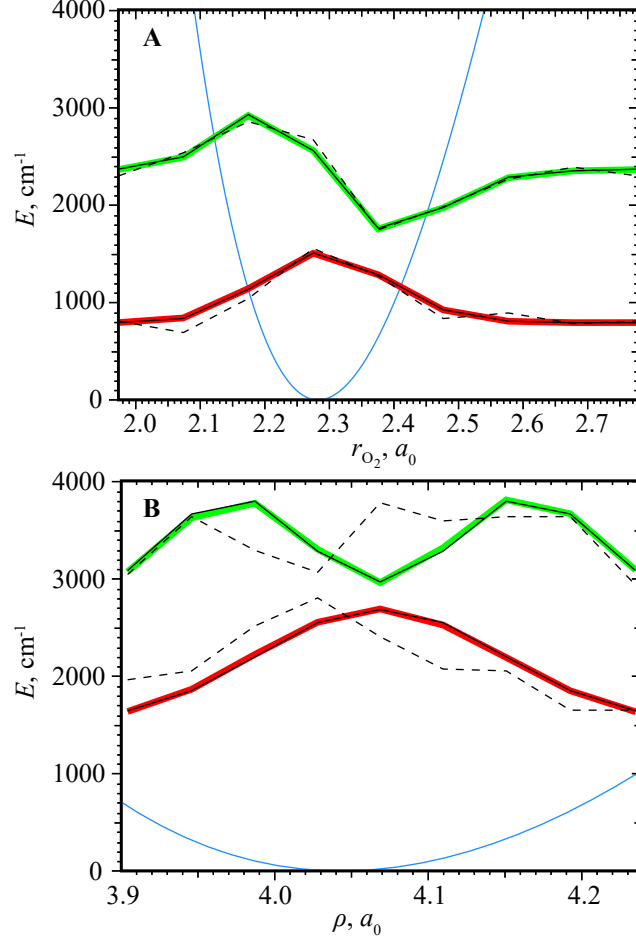


**Fig. 1. Computed wave functions of the ground and first excited states.** The molecules are (A)  $\text{O}_2$  and (B)  $\text{O}_3$ , the wave function is squared for ozone. Red and green bold curves are the results of a classical numerical eigensolver (LAPACK). Solid thin black curves were obtained using QAE with a software classical QUBO solver (they lie on top of the LAPACK curves). Dashed black curves are the results obtained using QAE with a hardware quantum annealer (D-Wave machine). The blue curve is (A) oxygen potential  $V(r_{\text{O}_2})$  and (B) minimum energy path for ozone.

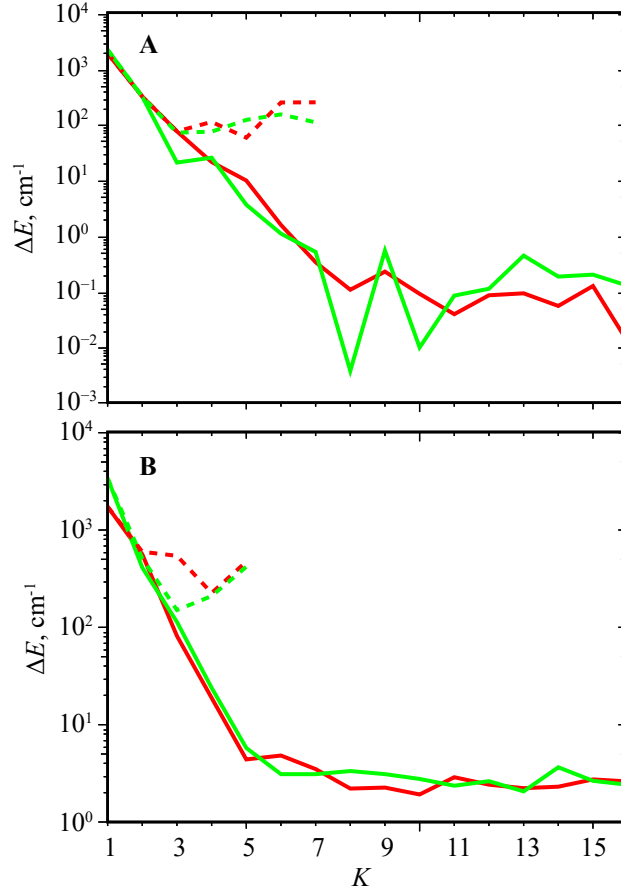


**Fig. 2.** Ground and first excited state energy errors as a function of number of qubits  $K$  per expansion coefficient  $a_\alpha$ . The molecules are (A)  $\text{O}_2$  and (B)  $\text{O}_3$ . Ground state is red, excited state is green. Results were obtained using QAE with a classical QUBO solver (solid curves) and a quantum annealer (dashed curves). Errors are computed relative to the energies of a classical numerical eigensolver (LAPACK).

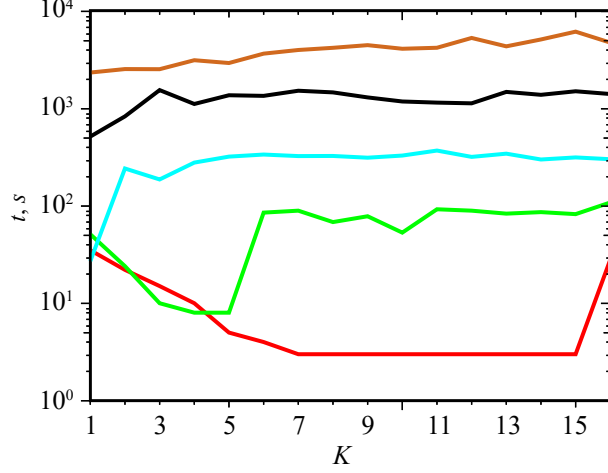


**Fig. 3. Normalized computational time for the  $d$ -dimensional harmonic oscillator.** The time is plotted as a function of  $K$  and was obtained using QAE with a classical QUBO solver. Results are presented for 1D (red), 2D (green), 3D (blue), 4D (black) and 5D (brown). Number of cosine basis function is  $B = 3$  ( $m_{max} = 2$ ). No slope in all curves demonstrates linear scaling of the algorithm with  $K$ .

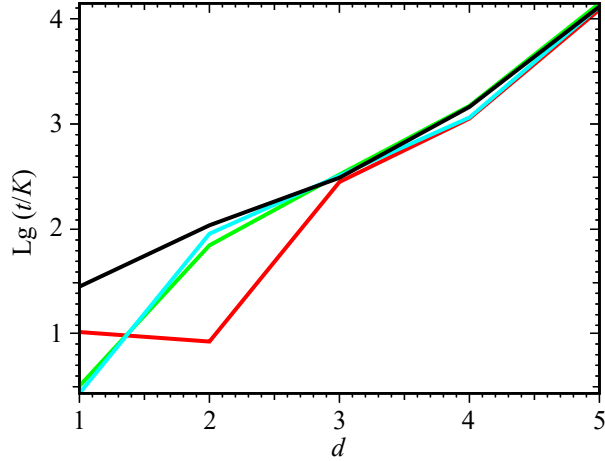


**Fig. 4. Logarithm of the normalized computational time as a function of the number of dimensions.** The time was measured for the  $d$ -dimensional harmonic oscillator and was obtained using QAE with a classical QUBO solver. Results are presented for the number of qubits per coefficient  $K = 4$  (red),  $K = 8$  (green),  $K = 12$  (blue) and  $K = 16$  (black). Number of cosine basis functions is  $B = 3$  ( $m_{max} = 2$ ). The linear dependence confirms exponential scaling in  $d$ .

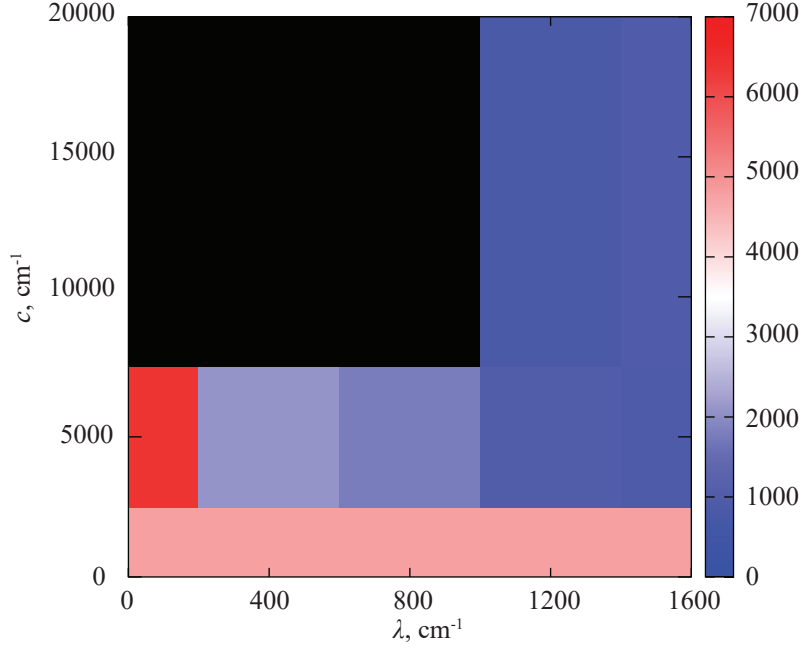


**Fig. 5. Scanning in the normalization  $\lambda$  and chain  $c$  penalties.** The calculation was performed on the hardware quantum annealer (D-Wave machine) to find the minimum energy (see color scale in  $\text{cm}^{-1}$ ). The three major regions of interest are: trivial solutions (top-left black), broken chains (bottom red-blue) and the optimal region where *both* the normalization and chain constraints are satisfied and the minimum energy solution is obtained (top-right blue).

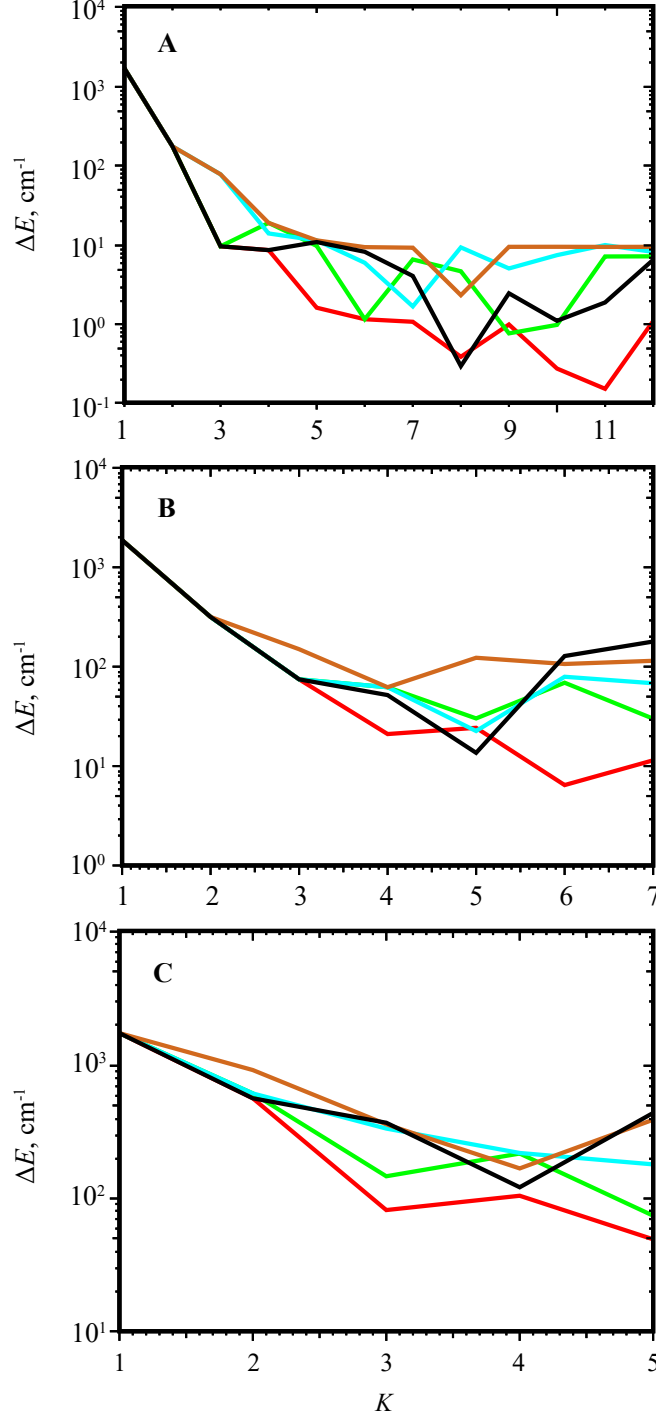


**Fig. 6. Simulation of quantum annealer noise.** (A) 1D harmonic oscillator, (B)  $O_2$  and (C)  $O_3$ . In each panel, the classical QUBO solution error (relative to LAPACK) is plotted as a function of the number of qubits  $K$  for different noise models. In general, the error for the quantum annealer (black curves) is larger than for the classical solver without noise (red curves). The quantum annealer behavior can be qualitatively reproduced by adding noise to the classical calculation. For the 1D harmonic oscillator and  $O_2$  the noise was added with scaling factors of 1 (green), 3 (blue) and 5 (brown). For  $O_3$  the noise scaling factors are 3 (green), 5 (blue) and 7 (brown).

## SUPPLEMENTARY MATERIALS

In this document we are addressing several important questions to support the findings of the main text. First of all, as it was mentioned in the subsection on algorithm scaling, the QUBO solver may also have some additional effects on performance. Figure S1 shows a step-like runtime as a function of  $K$  for the classical QUBO solver we used in this work (see Materials and Methods). The steps are caused by a backbone-based method inspired by Glover, *et al.* (38) used to decompose a large QUBO instance into smaller sub-QUBOs and further combining these to produce a solution of the large (original) QUBO problem. The QUBO problems which are smaller than the sub-QUBO size (the default is 47 or is defined by hardware) are solved directly and are extremely fast, resulting in a negligibly small runtime for small  $K$  in the figure. The steps become less distinguishable with increasing problem size.

Next, we report the primary results of the convergence studies for the QAE algorithm. All errors are computed relative to the energies of the classical numerical eigensolver LAPACK. In Figures S2-S4 convergence of the ground state energy is given for the molecules  $O_2$  and  $O_3$ , in addition to the dependence on number of qubits  $K$  discussed earlier in the main text (see Figure 2). The basis size is the same across all three figures. For  $O_2$ , the Fourier basis size is  $B = 9$  ( $m_{max} = 4$ ). For  $O_3$ , the SDT basis size is  $B = 12$  ( $E_{cut} = 2000 \text{ cm}^{-1}$ ). The analysis depends on the QUBO solver used in conjunction with QAE algorithm.

For the software based classical QUBO solver qbsolv (Tabu search with subspace iteration), the part of qbsolv which mostly influences convergence is the stopping criterion. This criterion is specified by the maximum number of repeats  $N_{rep}$  the solver has to perform without any improvement to the solution. Figure S2 demonstrates convergence as a function of  $N_{rep}$ . The number of qubits per coefficient is  $K = 8$  for both molecules. For the hardware based QUBO solver (D-Wave quantum annealer), the most sensitive parameter is the number of reads  $N_{reads}$  (number of annealing cycles). The convergence with respect to  $N_{reads}$  is shown in Figure S3. The number of qubits per coefficient is  $K = 7$  for  $O_2$  and  $K = 5$  for  $O_3$ . The dependence on other QUBO solver parameters, for example, the size of Tabu memory for qbsolv or annealing time for the D-Wave annealer was found to be negligible.

The parameter which is solver independent and is intrinsic to the algorithm itself is the



number of steps  $N_\lambda$  for the normalization penalty  $\lambda$ . Figure S4 illustrates the effect of  $N_\lambda$  on the energy errors. The scanning range of  $2000 \text{ cm}^{-1}$  was kept unchanged, whereas the step size  $\Delta\lambda$  was decreased. Increasing the  $\lambda$  resolution gives a better result. The initial  $\lambda$  is given in Table 1. The number of qubits per coefficient is the same as in Figure S2.

The last Figure S5 shows the convergence of the ground state energy error for the  $d$ -dimensional harmonic oscillator as a function of the number of qubits per expansion coefficient  $K$ . The cosine basis size is  $B = 3$  ( $m_{max} = 2$ ),  $B = 4$  ( $m_{max} = 3$ ) and  $B = 5$  ( $m_{max} = 4$ ). This benchmark calculation exhibits the same features observed in the calculations for the real systems  $\text{O}_2$  and  $\text{O}_3$  (see Figure 2). These features are an exponential drop of the error for small  $K$ , a plateau for large  $K$  and an increase of the error with problem size (both in the number of dimensions  $d$  and number of basis functions  $B$ ).

Finally, Table I summarizes parameters that we used to perform  $\lambda$  scanning for different ground state problems: initial value  $\lambda_{min}$ , number of steps  $N_\lambda$  and step size  $\Delta\lambda$ . As indicated in the last column, the step size must be significantly increased for small problem sizes to avoid trivial solution  $\Psi = 0$ . Parameters for first excited states of  $\text{O}_2$  and  $\text{O}_3$  are also given.

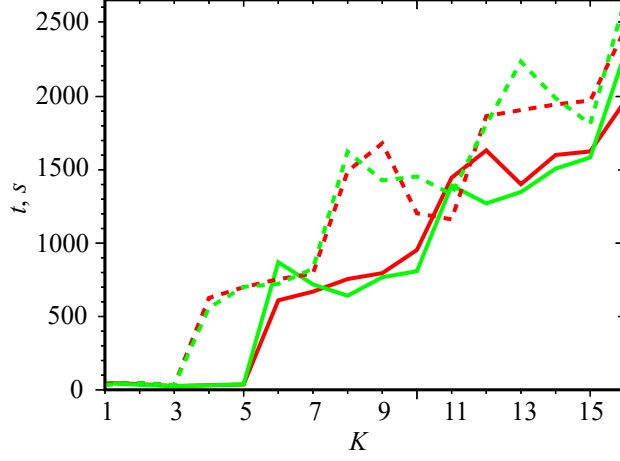


**Fig. S1.** Computational time using a classical QUBO solver. The molecules are  $O_2$  (solid lines) and  $O_3$  (dashed lines). Both ground (red curve) and first excited (green curve) states are shown.

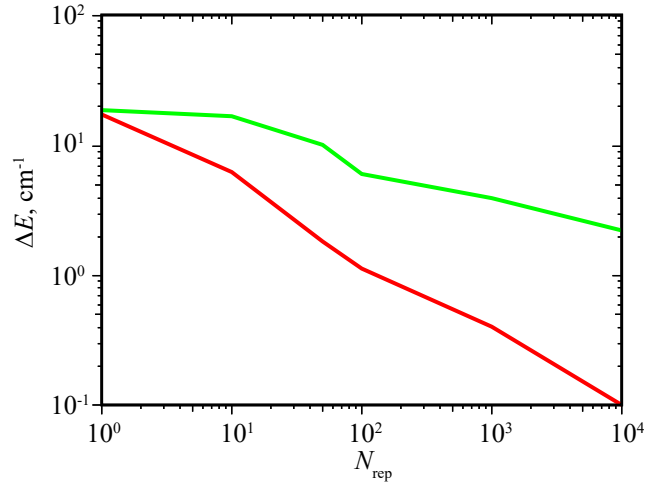


**Fig. S2.** Convergence of ground state energies with respect to the number of repeats  $N_{rep}$  in qbsolv stopping criterion. The molecules are  $O_2$  (red curve) and  $O_3$  (green curve). The classical QUBO solver was used.

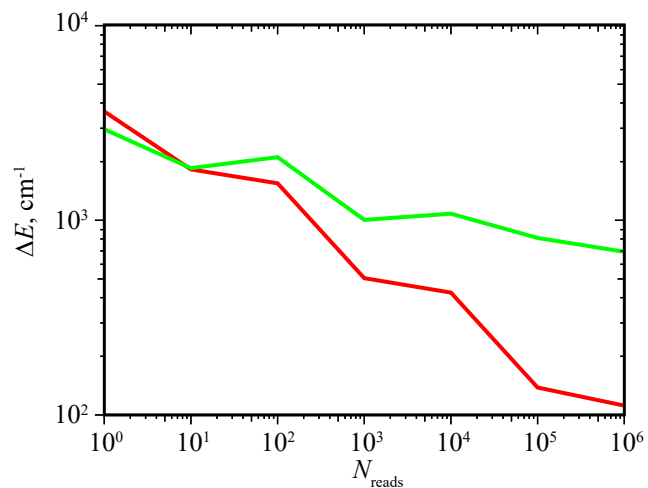


**Fig. S3.** Convergence of ground state energies with respect to the number of reads  $N_{\text{reads}}$  in the quantum annealer. The molecules are O<sub>2</sub> (red curve) and O<sub>3</sub> (green curve). D-Wave machine was used.

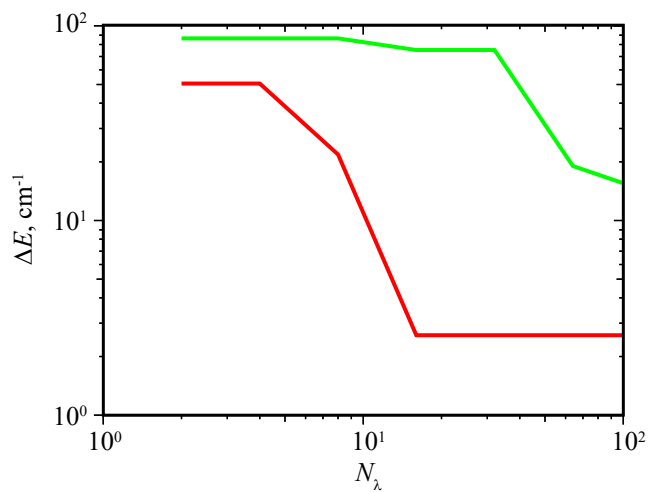


**Fig. S4.** Convergence of ground state energies with respect to the number of steps  $N_{\lambda}$ . The molecules are O<sub>2</sub> (red curve) and O<sub>3</sub> (green curve).  $\Delta\lambda$  was adjusted to keep the same scanning range. The classical QUBO solver was used.

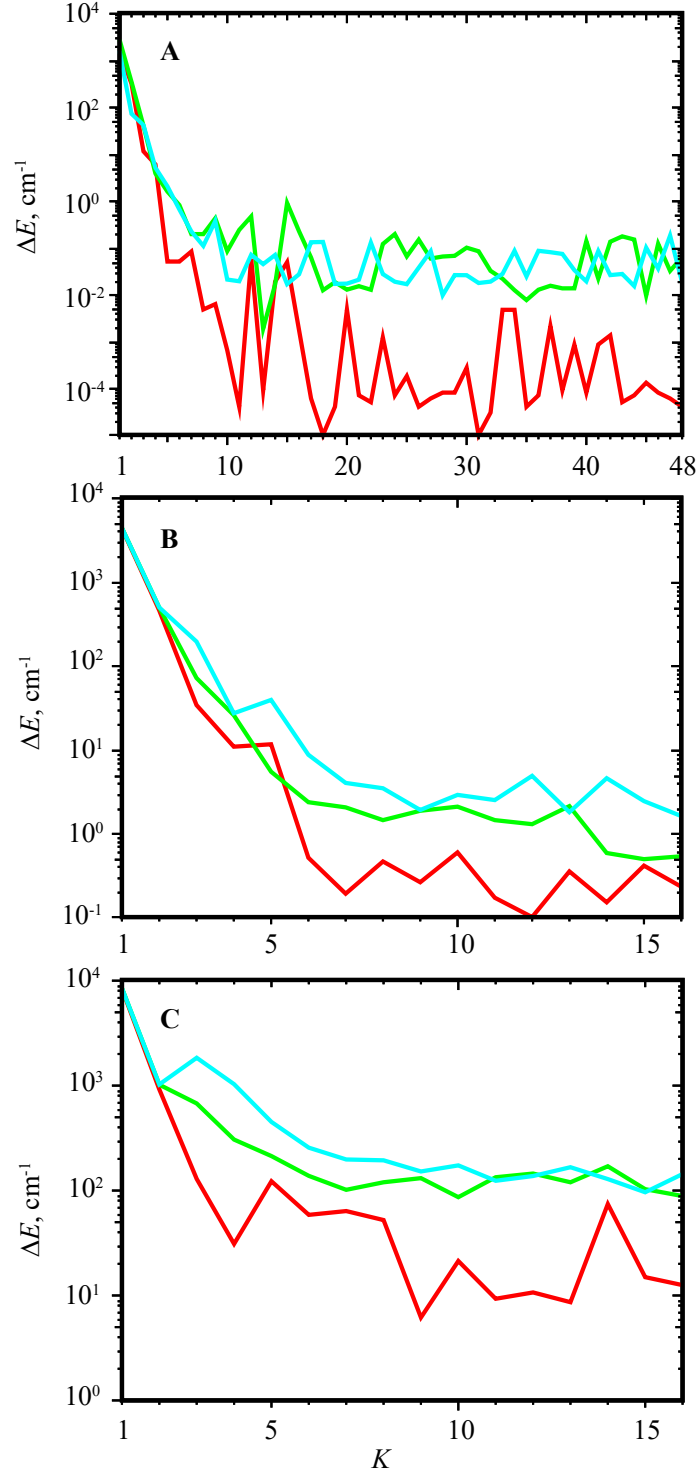


**Fig. S5.** Ground state energy error as a function of number of qubits  $K$  per expansion coefficient  $a_\alpha$ . Computed for (A) 1D, (B) 2D and (C) 3D harmonic oscillators. The number of cosine basis functions is  $B = 3$  (red),  $B = 4$  (green) and  $B = 5$  (blue). The classical QUBO solver was used.

**Table I. Parameters for normalization penalty  $\lambda$  in  $\text{cm}^{-1}$** 

Problem	$\lambda_{min}$	$N_\lambda$	$\Delta\lambda$	$\Delta\lambda$ for small $K$
O <sub>2</sub>	780	10	10	400 ( $K = 1$ ) and 200 ( $K = 2-4$ )
O <sub>2</sub> 1st excited	2350	10	10	800 ( $K = 1$ ) and 100 ( $K = 2$ )
O <sub>3</sub>	1560	10	10	400 ( $K = 1$ ) and 100 ( $K = 2-3$ )
O <sub>3</sub> 1st excited	2840	10	10	800 ( $K = 1$ ) and 100 ( $K = 2-3$ )
1D-harmonic	380	10	10	400 ( $K = 1$ ) and 200 ( $K = 2$ )
2D-harmonic	880	10	10	800 ( $K = 1$ ) and 100 ( $K = 2-3$ )
3D-harmonic	1580	10	10	800 ( $K = 1$ ) and 100 ( $K = 2-8$ )
4D-harmonic	3000	10	200	1600 ( $K = 1$ )
5D-harmonic	3000	10	500	3000 ( $K = 1$ )
1D-harmonic + noise	380	40	50	
O <sub>2</sub> + noise	780	40	50	
O <sub>3</sub> + noise	1560	40	50	